Title

High-Throughput Drug Screening Identifies a Potent Wnt Inhibitor that Promotes Airway Basal Stem Cell Homeostasis.

Journal

Cell reports, 30(7)

ISSN

2211-1247

Authors

Aros, Cody J
Paul, Manash K
Pantoja, Carla J
et al.

Publication Date

2020-02-01

DOI

10.1016/j.celrep.2020.01.059

Peer reviewed

HHS Public Access

Author manuscript

Cell Rep. Author manuscript; available in PMC 2020 March 02.

Published in final edited form as:

Cell Rep. 2020 February 18; 30(7): 2055–2064.e5. doi:10.1016/j.celrep.2020.01.059.

High-Throughput Drug Screening Identifies a Potent Wnt Inhibitor that Promotes Airway Basal Stem Cell Homeostasis

Cody J. Aros[1,2,3], **Manash K. Paul**[4], **Carla J. Pantoja**[3], **Bharti Bisht**[4], **Luisa K. Meneses**[3], **Preethi Vijayaraj**[3,5], **Jenna M. Sandlin**[3], **Bryan France**[7], **Jonathan A. Tse**[3], **Michelle W. Chen**[3], **David W. Shia**[1,2,3], **Tammy M. Rickabaugh**[3], **Robert Damoiseaux**[5,6,7], **Brigitte N. Gomperts**[2,3,4,5,8,9,*]

[1]UCLA Department of Molecular Biology Interdepartmental Program, UCLA, Los Angeles, CA 90095, USA

[2]UCLA Medical Scientist Training Program, David Geffen School of Medicine, UCLA, Los Angeles, CA 90095, USA

[3]UCLA Children's Discovery and Innovation Institute, Mattel Children's Hospital UCLA, Department of Pediatrics, David Geffen School of Medicine, UCLA, Los Angeles, CA 90095, USA

[4]Division of Pulmonary and Critical Care Medicine, David Geffen School of Medicine, UCLA, Los Angeles, CA 90095, USA

[5]Jonsson Comprehensive Cancer Center, UCLA, Los Angeles, CA 90095, USA

[6]UCLA Department of Molecular & Medical Pharmacology, UCLA, Los Angeles, CA 90095, USA

[7]California NanoSystems Institute, UCLA, Los Angeles, CA 90095, USA

[8]Eli and Edythe Broad Stem Cell Research Center, UCLA, Los Angeles, CA 90095, USA

[9]Lead Contact

SUMMARY

Mechanisms underpinning airway epithelial homeostatic maintenance and ways to prevent its dysregulation remain elusive. Herein, we identify that β-catenin phosphorylated at Y489 (p-β-catenin^{Y489}) emerges during human squamous lung cancer progression. This led us to develop a model of airway basal stem cell (ABSC) hyperproliferation by driving Wnt/β-catenin signaling, resulting in a morphology that resembles premalignant lesions and loss of ciliated cell

*Correspondence: bgomperts@mednet.ucla.edu.

AUTHOR CONTRIBUTIONS

C.J.A. contributed to conception and design, collection and assembly of data, data analysis and interpretation, and manuscript writing. M.K.P. and B.B. contributed to conception and design, collection and assembly of data, and data analysis and interpretation. C.J.P. contributed to collection and assembly of data, data analysis and interpretation, and technical support. P.V., L.K.M., J.M.S., B.F., J.A.T., M.W.C., and T.M.R. contributed to data analysis and interpretation and technical support. D.W.S. contributed to data analysis and interpretation. R.D. contributed to conception and design and data analysis and interpretation. B.N.G. contributed to conception and design, data analysis and interpretation, manuscript writing, final approval of the manuscript, and financial support.

SUPPLEMENTAL INFORMATION

Supplemental Information can be found online at https://doi.org/10.1016/j.celrep.2020.01.059.

DECLARATION OF INTERESTS

A patent has been filed on the contents of this manuscript.

differentiation. To identify small molecules that could reverse this process, we performed a high-throughput drug screen for inhibitors of Wnt/β-catenin signaling. Our studies unveil Wnt inhibitor compound 1 (WIC1), which suppresses T-cell factor/lymphoid enhancer-binding factor (TCF/LEF) activity, reduces ABSC proliferation, induces ciliated cell differentiation, and decreases nuclear p-β-catenin^{Y489}. Collectively, our work elucidates a dysregulated Wnt/p-β-catenin^{Y489} axis in lung premalignancy that can be modeled *in vitro* and identifies a Wnt/β-catenin inhibitor that promotes airway homeostasis. WIC1 may therefore serve as a tool compound in regenerative medicine studies with implications for restoring normal airway homeostasis after injury.

Graphical Abstract

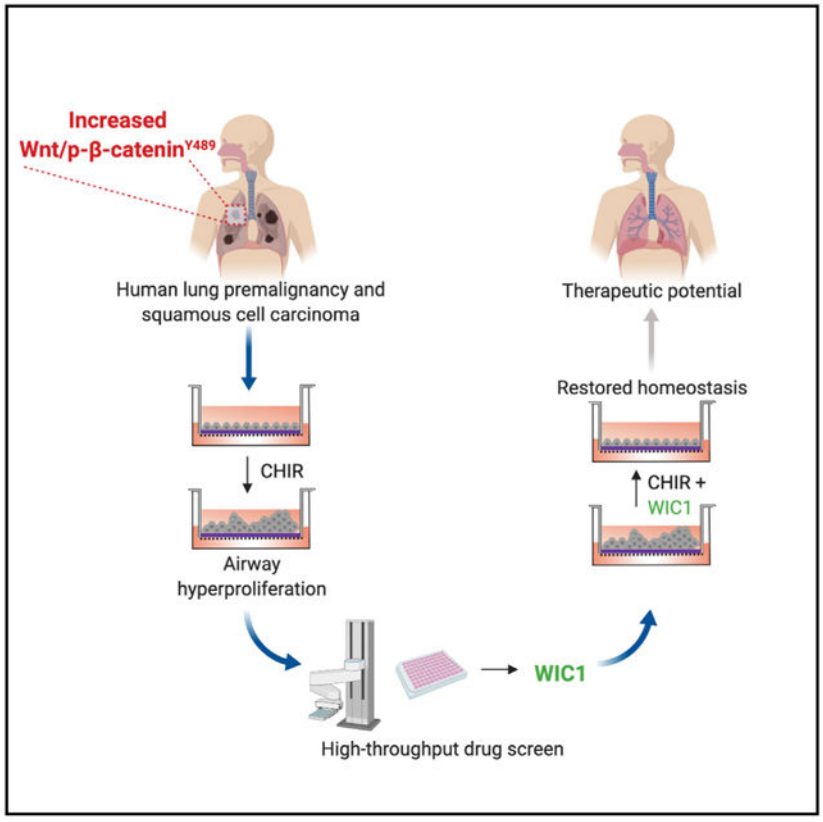

In Brief

Aros et al. unveil a dysregulated Wnt/β-catenin signaling axis in lung premalignancy that can be modeled *in vitro*. They leverage this knowledge to conduct a drug screen and identify a small-molecule inhibitor of Wnt/β-catenin signaling that restores airway epithelial homeostasis.

INTRODUCTION

The conducting airways play a vital role in host defense that protects mammals from airborne pathogens. This is accomplished by a specialized pseudostratified mucociliary epithelium that arises from anatomically defined, resident adult airway basal stem cells (ABSCs) marked by keratin 5 (K5) expression (Cole et al., 2010; Hong et al., 2004;

Montoro et al., 2018; Plasschaert et al., 2018; Rock et al., 2009; Schoch et al., 2004). Following injury, the tracheal repair response occurs in two distinct phases: initial epithelial denuding triggers ABSC proliferation, followed by a phase of differentiation. This ultimately leads to epithelial repair with the optimal proportion of ABSCs and mucociliary cells. Dysregulated repair can lead to various pathologies, including ABSC hyperplasia and stepwise progression to squamous lung cancer (SqLC) (Hogan et al., 2014; Ooi et al., 2010). As such, developing a nuanced understanding of the mechanisms governing ABSC homeostasis is paramount to making strides in improving clinical outcomes for patients with lung diseases.

The canonical Wnt/β-catenin signaling cascade, although previously implicated in modulating airway homeostasis (Giangreco et al., 2012; Zemke et al., 2009), remains poorly understood. We therefore sought to elucidate the biology that underlies airway homeostasis maintenance and to identify small molecules that could potentially restore dysregulated homeostasis, thereby informing clinically relevant interventions for lung diseases.

RESULTS

Emergence of Dysregulated Wnt/p-β-Catenin^{Y489} Signaling Axis in Stepwise Progression to Human SqLC

SqLC is thought to arise from excessive proliferation of K5+ ABSCs and progress through a series of histologically-defined premalignant intermediates as a product of dysfunctional homeostatic mechanisms (Ishizumi et al., 2010). Further, β-catenin post-translational modifications have been shown to regulate its subcellular localization and signaling in other contexts (Fang et al., 2007; Huber and Weis, 2001; Rhee et al., 2007). To determine whether Wnt/β-catenin signaling is dysregulated during human SqLC progression, we performed immunofluorescence (IF) staining and analysis on human patient airway samples for varying pathway components. In contrast to its nuclear expression in only 5.2% of histologically normal human airway epithelia, β-catenin phosphorylated at Y489 (p-β-catenin^{Y489}) uniquely localized to the nucleus in 35.7% of human airway premalignant lesions (PMLs) and 50.9% of SqLC patient samples (Figures 1A and 1B). Further, while only 7.2% of basal cells from normal human patient airways contained nuclear p-β-catenin^{Y489}, 38.3% and 62.7% of ABSCs exhibited nuclear p-β-catenin^{Y489} in PMLs and SqLCs, respectively (Figure 1C). These findings stood in contrast to other phosphorylated forms of β-catenin that only localized to the membrane or cytoplasm (Figures S1A–S1C).

Utilizing Porcupine IF staining as an indicator of Wnt secretion by airway cells (Tammela et al., 2017), we additionally observed minimal epithelial and no stromal expression of Porcupine in normal human airways (Figures 1D and 1E). However, Porcupine was expressed in the epithelium of 50% and 100% of PMLs and SqLC samples analyzed, respectively (Figure 1E). We further quantified the percentage of ABSCs that were also Porcupine^{+} in these samples. While 5.8% of ABSCs were Porcupine^{+} in normal human airways, this increased to 34.8% and 70.1% of ABSCs in PML and SqLC patient samples (Figure 1F). We also observed Porcupine staining in the stromal compartment during stepwise progression to SqLC (Figure 1D). While zero of the five normal human airways examined had positive stromal Porcupine staining, 16.7% PMLs and 62.5% SqLCs

displayed positive stromal Porcupine expression (Figure 1G). Consistent with these findings, 7.2% of stromal cells in PMLs and 24.3% of stromal cells in SqLCs were also Porcupine^{+} (Figure 1H). These studies collectively elucidate the emergence of a dysregulated Wnt/p-β-catenin^{Y489} signaling axis during stepwise progression to human SqLC.

ABSC Homeostasis Is Controlled by Perturbations in Canonical Wnt Signaling *In vitro*

To determine whether the pathobiology observed in human patients can be modeled *in vitro*, we first isolated and seeded mouse ABSCs (mABSCs) in collagen-coated transwells. On day 1, mABSCs were then treated with the GSK3β inhibitor CHIR99021 (CHIR) under submerged culture conditions until day 4 to activate canonical Wnt signaling (Figure 2A). We performed EdU (5-ethynyl-2′-deoxyuridine) proliferation assays from mABSCs treated with CHIR and observed statistically significant increased ABSC proliferation in comparison to DMSO-treated controls (Figures 2B and 2C).

We next inquired whether there were changes in the ability of ABSCs to differentiate to the ciliated cell fate *in vitro* following Wnt activation. To this end, mABSCs were isolated and treated with CHIR under submerged culture conditions for 4 days as shown in the schematic presented in Figure 2D. On day 4, media from the apical chambers were removed, and mABSCs were cultured under air-liquid interface (ALI) differentiation conditions with CHIR until day 14 (Figure 2D). Strikingly, mABSCs treated with CHIR exhibited a dose-dependent heaping morphology that resembles the PMLs seen in the airways of patients (Figure 2E). Further, mABSCs treated with two independent GSK3β inhibitors (CHIR and GSK3XV) displayed a significant reduction in the percentage of ciliated cells, indicated by the absence of acetylated β-tubulin, and an increased pool of K5^{+} mABSCs (Figures 2F and 2G). We additionally observed that human ABSCs (hABSCs) treated with CHIR for 21 days (Figure S2A) similarly exhibited abolished differentiation to the ciliated cell fate and an increased pool of ABSCs (Figures S2B and S2C).

We next sought to determine the extent of Wnt/β-catenin signaling activation upon dysregulated ABSC homeostasis by performed IFs on mABSC cultures treated with CHIR. We observed increased nuclear p-β-catenin^{Y489} relative to DMSO-treated control cultures (Figure 2H). In contrast, other phosphorylated forms of β-catenin (p-β-catenin^{Y654}, p-β-catenin^{S552}, and p-β-catenin^{S33,S37,T41}) remained primarily cytoplasmic or membranous in the submerged phase of culture (Figures S2D–S2G). Additionally, GSK3β inhibition and recombinant Wnt3a increased TCF/LEF activity measured by a luciferase reporter in comparison to DMSO-treated cultures (Figure 2I). To assess the possibility that differing levels of Wnt signaling could produce phenotypic differences *in vitro*, mABSCs were treated with varying concentrations of recombinant Wnt3a under ALI conditions. Interestingly, we observed that medium levels of Wnt signaling (100 ng/mL) increased the proportion of ciliated cells, while high levels of Wnt signaling (500 ng/mL) produced fewer ciliated cells at the expense of K5^{+} mABSC expansion (Figures 2J and 2K). Collectively, our results demonstrate that ABSC homeostasis is controlled by perturbations in canonical Wnt signaling, and we have developed a tractable system in which we can monitor the biology underlying ABSC hyperplasia.

High-Throughput Drug Screening Identifies a Small-Molecule Inhibitor of Canonical Wnt Signaling

In light of our findings that Wnt/β-catenin signaling drives ABSC hyperproliferation, we sought to identify small-molecule inhibitors of the pathway that could restore airway homeostasis. To this end, we conducted a high-throughput drug screen that would decrease Wnt/β-catenin signaling activity and ABSC proliferation (Figure 3A). BEAS2B cells, a normal human bronchial epithelial cell line, were transduced to stably express a TCF/LEF luciferase reporter that could be induced by treatment with CHIR after 24 h (Figure 3B). The Z′ factor for this screen was calculated to be 0.82, indicating a reliable platform to identify target compounds. BEAS2B cells were treated with DMSO, 5 μM CHIR, or 5 μM CHIR + 10 μM screen compound for 24 h, after which TCF/LEF activity was measured. Hoechst staining was also conducted in parallel to assess for toxicity. Compounds that yielded fewer than 80% of nuclei compared to DMSO controls by Hoechst staining were considered toxic and removed from further analysis. We screened 20,000 small molecules and initially identified 70 compounds that decreased TCF/LEF activity, 8 of which were nontoxic, and 4 compounds that exhibited dose dependence. Compounds A–C reproducibly decreased TCF/LEF activity and were nontoxic by CellTiter-Glo measurements (Figures S3A–S3F) but did not modulate ABSC proliferation (data not shown). However, Wnt inhibitor compound 1 (WIC1) was a small molecule that decreased TCF/LEF luciferase reporter activity (Figure 3C) and displayed no toxicity by Hoechst stain (Figure 3D). Further, BEAS2B cells treated with a dose course of WIC1 for 24 h showed a stepwise decrease in TCF/LEF activity (Figure 3E) and remained nontoxic even at 10 μM, as measured by the CellTiter-Glo assay (Figure 3F).

In light of the structure of WIC1 (Figure 3G), we conducted structure-activity relationship (SAR) studies with an additional 160 small molecules that bore structural resemblance to WIC1. We conducted TCF/LEF luciferase dose-course assays with these compounds and identified 8 additional small molecules that reproducibly decreased reporter activity, named WIC2–WIC9 (Figures 3H and S3G). Analysis of the compound hits WIC2–WIC9 from our SAR study indicated a common dihydrocoumarin pharmacophore that was substituted with a carboxy moiety in 3 position that in turn was conjugated to a moiety that had an aniline as maximum common substructure. Together, our results reveal members of a well-known, important pharmacophore for which we have identified a role in modulating canonical Wnt signaling.

As recent studies have identified Wnt inhibitors that mechanistically act at varying levels of the pathway (Fang et al., 2016; Hwang et al., 2016), we measured and compared BEAS2B TCF/LEF luciferase reporter activity following 24 h of treatment with 5 μM CHIR or 5 μM CHIR plus a dose course of WIC1 against other published Wnt inhibitors MSAB, LF3, and ICG001. We observed that while MSAB was the only inhibitor that decreased TCF/LEF activity at 10 nM, WIC1 remained the most potent inhibitor at 100 nM and 1 μM (Figure 3I). Further, all Wnt inhibitors assayed, except WIC1, were toxic at higher concentrations, as measured by CellTiter-Glo (Figure 3J). These data collectively indicate that WIC1 is a more potent Wnt inhibitor across a wider range of concentrations at which other known Wnt inhibitors display cellular toxicities.

WIC1 Inhibits Wnt-Induced ABSC Hyperproliferation, Promotes Ciliated Cell Differentiation, and Acts by Decreasing Nuclear p-β-Catenin^{Y489}

To assess whether WIC1 could reverse Wnt/β-catenin-induced primary ABSC hyperproliferation, we treated hABSCs with DMSO, CHIR, or CHIR + WIC1 under submerged conditions for 4 days. Cultures treated with CHIR + WIC1 displayed a significant reduction in ABSC proliferation measured by EdU incorporation (Figures 4A and 4B). We next sought to understand if WIC1 could promote ABSC differentiation to ciliated cells under ALI conditions. Relative to DMSO controls, mABSC cultures treated with 100 nM WIC1 significantly induced ciliated cell differentiation (Figures 4C and 4D). Interestingly, however, higher concentrations of WIC1 (1 μM) decreased the percentage of ciliated cells in culture (Figures 4C and 4D), consistent with our observations that tightly regulated levels of Wnt signaling are critical for proper regulation of airway homeostasis (Figures 2J and 2K).

We next inquired how the effects of WIC1 on ABSC proliferation and differentiation compared to the Wnt inhibitors MSAB, LF3, and ICG001. To this end, we treated mABSCs under submerged culture conditions for 4 days with DMSO, 1 μM CHIR, and 1 μM CHIR + 1 μM WIC1, 1 μM MSAB, 1 μM LF3, or 1 μM ICG001. We observed that cultures treated with CHIR and all of the Wnt inhibitors, including WIC1, decreased mABSC proliferation to a similar degree, as measured by EdU incorporation (Figures S4A and S4B). These data indicate that WIC1 regulates ABSC proliferation in a manner similar to other known Wnt signaling inhibitors. Additionally, we performed ALI differentiation assays with mABSCs treated with DMSO and two different concentrations (100 nM and 1 μM) of WIC1, MSAB, LF3, or ICG001. These studies revealed that 100nM of WIC1, LF3, and ICG001 induced a greater proportion of ciliated cells under ALI conditions in comparison to DMSO-treated cultures (Figures S4C and S4D). However, treatment with 1 μM WIC1, LF3, or ICG001 had no effect on the percentage of ciliated cells in culture (Figures S4C and S4D). Interestingly, neither 100 nM nor 1 μM MSAB increased differentiation to the ciliated cell fate (Figures S4C and S4D). Taken together, our findings illustrate that low-dose WIC1 acts in a similar fashion to a subset of other known Wnt inhibitors in promoting ciliogenesis.

To develop an understanding of the mechanism by which WIC1 modulates Wnt signaling, we first performed qRT-PCR to assess target gene expression in the context of BEAS2B cells treated with DMSO, 5 μM CHIR, or 5 μM CHIR + 1 μM WIC1. While we observed a notable increase in mRNA expression of known downstream Wnt signaling target genes *CCND1*, *MYC*, and *CTNNB1* with CHIR treatment, addition of WIC1 to these cultures resulted in a significant decrease in their expression (Figure 4E). Moreover, recent work by Haas et al. demonstrated that high levels of Wnt/β-catenin signaling activate ΔN-TP63 expression to promote basal cell proliferation (Haas et al., 2019). As such, we first sought to understand whether treatment with WIC1 under settings of high Wnt signaling could modulate expression of *TP63*. qRT-PCR studies from RNA isolated from BEAS2B cells identified an increase in *TP63* expression with the addition of CHIR that was reduced upon addition of WIC1 (Figure S4E). Further, RNA was also isolated from primary mABSC cultures on day 9 of ALI, and we found induction of *Trp63* expression with CHIR treatment that was substantially reversed with WIC1 treatment (Figure 4F). To further dissect the

mechanism by which WIC1 acts, we next assessed its effect on phosphorylation of β-catenin at Y489. To this end, we treated BEAS2B cells for 24 h with DMSO, 5 μM CHIR, or 5 μM CHIR + 1 μM WIC1. Strikingly, while CHIR treatment induced nuclear localization of p- β-catenin^{Y489}, addition of WIC1 to cultures abolished its nuclear localization (Figures 4G and 4H). Taken together, these data offer insight that WIC1 modulates its phenotypic effects on airway homeostasis, in part, via TP63/p-β-catenin^{Y489}-dependent mechanisms.

DISCUSSION

Here, we identified a phosphorylated form of β-catenin that becomes activated in human patients during excessive ASBC proliferation in premalignancy and stepwise progression to SqLC. We further demonstrated that gradient levels of Wnt signaling can result in loss of ABSC homeostasis that can be modeled *in vitro*. We leveraged this knowledge to conduct high-throughput drug screening that revealed an unannotated small-molecule inhibitor of Wnt/β-catenin signaling, WIC1. Importantly, the ability of WIC1 to restore airway homeostasis by preventing ABSC hyperproliferation and improving differentiation to the ciliated cell fate has implications for use in other airway diseases with poor mucociliary clearance, such as COPD. Our work and others highlight how high-throughput drug screening can serve as an instrumental platform to identify targetable biology and therapeutic compounds to treat diseases (Gerby et al., 2016; Lyou et al., 2017).

Prior studies unveiled that β-catenin is dispensable in the bronchiolar airways for homeostasis and injury repair (Zemke et al., 2009), while others affirmed that it may play a role in specification of mucus and ciliated cells *in vitro* (Malleske et al., 2018). In the proximal airway, we find that medium levels of Wnt/β-catenin signaling promote differentiation to the ciliated cell fate, consistent with work of others that has molecularly dissected a role for Wnt/β-catenin in regulating Foxj1-driven ciliogenesis across several species (Caron et al., 2012; Walentek et al., 2012, 2015). In contrast, however, excessive activation of Wnt/β-catenin signaling drives basal cell expansion. Further, low doses of the Wnt inhibitors WIC1, LF3, and ICG001 facilitate differentiation to the ciliated fate, while higher concentrations appear to have no effect. Our work has dissected the functional significance of how different levels of signaling yield differences in phenotypic effects of ABSC proliferation and differentiation to the ciliated cell fate. Our findings therefore underscore critically important, region-specific differences that are sensitive to concentration gradients.

Interestingly, Haas et al. recently highlighted that high levels of Wnt/β-catenin signaling activate ΔN-TP63 to serve as a key regulator of stemness by inhibiting differentiation to the ciliated cell fate (Haas et al., 2019). Our studies complement and extend these findings by identifying a key post-translational modification on β-catenin at Y489 that is uniquely associated with the nucleus in proliferating ABSCs, suggesting there might be a molecular link between TP63 and p-β-catenin^{Y489}. We have also identified a canonical Wnt/β-catenin signaling inhibitor that can restore airway epithelial homeostasis. Our work indicating decreased *TP63* expression and loss of nuclear p-β-catenin^{Y489} upon WIC1 treatment can, in part, explain the mechanism by which WIC1 facilitates differentiation to the ciliated cell fate.

Previous studies have also identified activation of an autocrine canonical Wnt signaling network in human non-small lung cancers (Akiri et al., 2009), consistent with our studies indicating that high levels of Wnt signaling abolish differentiation to the ciliated cell fate and promote ABSC expansion. Prior work demonstrating the presence of TP63 in human squamous lung tumors (Au et al., 2004; Ma et al., 2015; Wang et al., 2002) is likely, in part, driven by high levels of canonical Wnt signaling. Dysregulated Wnt signaling is likely accompanied by other signaling and genetic perturbations that further facilitate proximal airway remodeling and subsequent ABSC transformation (Haas et al., 2019). While malignancies from other organs such as colon have high rates of mutational burden in the Wnt signaling pathway, this is not true of lung malignancies (Ueda et al., 2001). Our data offer the insight that the Wnt signaling pathway may be perturbed at the level of post-translational modifications that would otherwise escape detection by RNA-sequencing technologies, as p-β-catenin^{Y489} emerges during stepwise progression to SqLC. Our studies also highlight the emergence of a stromal Wnt-producing niche during stepwise progression to SqLC.

While our studies indicate the functional significance of canonical Wnt/β-catenin signaling in modulation of airway basal stem cell homeostasis that was inspired by pathological findings from human patients, much remains to be learned about the heterogeneity in Wnt production and Wnt responsiveness of ABSCs. Analyses of SqLC biology at single-cell resolution can provide further insight into disease heterogeneity. Future studies should also address the functional role of Wnt signaling in the context of cellular niches in the regulation of airway homeostasis, regeneration, and disease processes, as this may unveil more specific, targetable biology.

STAR★METHODS

Detailed methods are provided in the online version of this paper and include the following:

LEAD CONTACT AND MATERIALS AVAILABILITY

Further information and requests for resources and reagents should be directed to and will be fulfilled by lead contact, Brigitte Gomperts (bgomperts@mednet.ucla.edu). This study did not generate unique reagents.

EXPERIMENTAL MODEL AND SUBJECT DETAILS

Mice—6-10-week-old male and female C57BL/6J wild-type mice were purchased from The Jackson Laboratory (Bar Harbor, Maine). Mice were maintained in a pathogen-free facility at the Division of Laboratory Animal Medicine (DLAM) at UCLA. Experiments were conducted in accordance with the guidelines by the DLAM Committee on Animal Care. All animal studies were approved by the UCLA Animal Research Committee and the UCLA Institutional Animal Care and Use Committee.

Human Tissue Procurement—Large airways and bronchial tissues were acquired from de-identified normal human donors after lung transplantations at the Ronald Reagan UCLA Medical Center. Tissues were procured under Institutional Review Board-approved protocols

at the David Geffen School of Medicine at UCLA. Information about age and sex of human samples are not available as they are de-identified.

METHOD DETAILS

Transient Transfections of mABSCs with TCF/LEF Luciferase Reporter— mABSCs were seeded in a 6-well transwell plate and transiently transfected with 0.8 μg of the TOPFLASH luciferase reporter and 0.8 μg Renilla Luciferase reporter vector pRL-TK for internal control (Promega). Transfections were conducted using Lipofectamine 2000 Transfection Reagent (ThermoFisher 11668030) following the manufacturer's protocol.

Generation of BEAS2B Cells with Stable Expression of TCF/LEF Luciferase Reporter—BEAS2B cells (ATCC CRL-9609) were seeded in a 6-well plate and infected with Cignal lentiviral particles containing a TCF/LEF luciferase reporter (QIAGEN CLS-018L). Cells were spin infected at 37°C for one hour using a multiplicity of infection of 20. Cells were selected with 0.6 μg/mL puromycin to isolate stably expressing clones.

High-throughput Drug Screening—A high-throughput drug screen was established to identify compounds capable of reducing TCF/LEF activity measured by a luciferase reporter induced by CHIR treatment in a 384-well format. Briefly, white-bottom 384-well plates (Greiner One) were precoated overnight with 0.01 mg/mL fibronectin from human plasma (Sigma F0895), 0.03mg/mL rat tail collagen type I (Corning 354249), and 0.01mg/mL BSA (ThermoFisher BP-9706) diluted in 50uL of Airway Epithelial Cell Growth Medium (PromoCell C21060). Precoat was then aspirated and washed using 100 μL the BioTek EL406. A custom V&P pin tool mounted to a Beckman FX liquid handler was then used to pin 0.5 μL of 10mM stock compound. 2,000 BEAS2B cells per well were then seeded using the Multidrop. Cells were treated with 1% DMSO, 5 μM CHIR, or 5 μM CHIR + 10 μM pinned compound and incubated for 24 hours at 37°C and 5% CO_2. 5 μg/mL Hoechst 33342 was added to each well, incubated for 15 minutes, and wells were visualized using the ImageXpress XL system. 25 μL BrightGlo (Promega) was subsequently added to each well using the BioTek EL405 and incubated for 2 minutes prior reading luminescence values with the Envision plate reader. We performed morphometric measurements by counting Hoechst-labeled cell nuclei per well. These data and BrightGlo luminescence data were uploaded into our Collaborative Drug Discovery (CDD) cloud-based database system (Ekins and Bunin, 2013). Hits were selected on a cut-off of more than 3 standard deviations from mean using data normalized to reference CHIR-treated wells within each plate. Z' factor values were used to assess assay quality and was calculated by: Z' = 1–3(SDTotal+SDBackground)/(Mean-Total− MeanBackground) (Inglese et al., 2006), where SDTotal and MeanTotal are the standard deviation and mean of signal for CHIR-treated wells, and SDBackground and MeanBackground are the standard deviation and mean of signal for DMSO-treated wells. We calculated the Z' factor value to be 0.82.

Luciferase Reporter Measurement—For luciferase reporter assays conducted outside of the high-throughput drug screen, BEAS2B cells were seeded in a 96-well plate at 15,000 – 20,000 cells per well. The following day, cells were with treated DMSO, 5 μM CHIR99021 (CHIR; Tocris 4423), 5 μM CHIR plus either WIC1, WIC2-WIC9, MSAB,

LF3, or ICG001 for 24 hours. Lysis reactions were conducted using BrightGlo (Promega E1910) and incubated for two minutes at room temperature prior to transferring luminescence reactions to white-bottom, white-walled 96-well plates (Costar). Toxicity assays were conducted by adding Cell Titer Glo reagent (Promega) following manufacturer's protocol. Luminescence readings were conducted using the Clariostar plate reader.

ABSC Isolation and Fluorescence-Activated Cell Sorting (FACS)—Mouse and human ABSCs were isolated following a previously published method by our laboratory (Hegab et al., 2012a; Hegab et al., 2014; Hegab et al., 2012b; Paul et al., 2014). Briefly, mouse tracheas were dissected, cleaned, and incubated in 16U/mL dispase for 30 minutes (1 hour for human) at room temperature. Tracheas were then incubated in 0.5mg/mL DNase for another 30 minutes (1 hour for human) at room temperature. Epithelium was stripped and incubated in 0.1% Trypsin-EDTA for 30 minutes (1 hour for human) shaking at 37°C to generate a single cell suspension. Isolated cells were passed through a 40 μm strainer and stained with fluorophore-conjugated antibodies against ITGA6 and TROP2. ITGA6+ TROP2+ cells were obtained via FACS that was completed using the BD FACSAria cell sorter.

Air-Liquid Interface (ALI) Cultures and *In vitro* Treatments—24-well 6.5mm transwells with 0.4 μm pore polyester membrane inserts were coated with 0.2mg/mL collagen type I dissolved in 60% ethanol and allowed to air dry. ABSCs were seeded at 100,000 cells per well and allowed to grow in the submerged phase of culture for 4–5 days with 500 μL media in the basal chamber and 200 μL media in the apical chamber. ALI cultures were then established and culture with only 500 μL media in the basal chamber, and cultures harvested at varying time points for immunofluorescence studies. Media was changed every other day and cultures were maintained at 37°C and 5% CO_2. ABSCs were treated with the indicated concentrations of GSK3XV, recombinant Wnt3a, CHIR, WIC1, MSAB, LF3, or ICG001.

Mouse Tracheal Epithelial Cell (MTEC) Plus and Serum-Free Media—Mouse and human ABSCs were grown in MTEC Plus media and MTEC serum-free media during the submerged and ALI phases of culture, respectively. MTEC base media is DMEM/Ham's F12 50/50 (Corning 15090CV). The tables below indicate the media components and concentrations for MTEC Plus and MTEC serum-free media.

MTEC Plus Media Formulation

Component	Concentration
HEPES (Sigma H0887)	15mM
Sodium Bicarbonate (Life Technologies 25080–094)	3.6mM
L-glutamine (Invitrogen 35050–061)	4mM
Insulin (Sigma I6634)	10 μg/mL
Transferrin (Sigma T5391)	5 μg/mL
Cholera Toxin (C8052)	0.1 μg/mL

Component	Concentration
Epidermal Growth Factor (Corning 354001)	25ng/mL
Bovine Pituitary Extract (Invitrogen 12028–014)	30 μg/mL
Fetal Bovine Serum (ThermoFisher SH3008003HI)	5%
Retinoic Acid (Sigma R2625)	0.05 μM

MTEC Serum-Free Media Formulation

Component	Concentration
HEPES	15mM
Sodium Bicarbonate	3.6mM
L-glutamine	4mM
Insulin	5 μg/mL
Transferrin	5 μg/mL
Cholera Toxin	0.025 μg/mL
Epidermal Growth Factor	5ng/mL
Bovine Pituitary Extract	30 μg/mL
Bovine Serum Albumin (ThermoFisher BP9706)	1mg/mL
Retinoic Acid	0.05 μM

In vitro* EdU Proliferation Assays—In vitro* proliferation was studied using the Click-iT EdU incorporation assay kit (Invitrogen C10337) following the company's protocol. Briefly, mouse and human ABSC cultures were treated with 10 μM EdU 6–8 hours prior to commencing IFs. Cells were fixed with 4% paraformaldehyde for 15 minutes followed by permeabilization in 0.5% Triton-X for 20 minutes. EdU cocktail was incubated for 30 minutes in darkness followed by immunocytochemistry.

Immunocytochemistry—Mouse and human ABSCs were fixed in 4% paraformaldehyde for 15 minutes followed by permeabilization with 0.5% Triton-X for 10 minutes. Cells were blocked using serum-free protein block (Dako X090930) for one hour at room temperature and overnight primary antibody incubation. Secondary antibodies were incubated for 1 hour in darkness, washed, and mounted using Vectashield hardest mounting medium with DAPI (Vector Labs H-1500). IF images were obtained using an LSM780 or LSM880 Zeiss confocal microscope and composite images generated using Fiji. The list of antibodies used is provided in the Key Resources Table as part of STAR Methods.

Immunofluorescence (IF)—4–5 μm thick paraffin-embedded sections were deparaffinized by placing them on a 60°C heating block for 1–2 hours and through a series of Xylene and ethanol washes. Antigen retrieval was then performed using a pressure cooker for 10 minutes in 1mM EDTA. Samples were permeabilized with 0.5% Triton-X, blocked using serum-free protein block (Dako X090930) for one hour, and incubated in primary antibody overnight. Secondary antibodies were incubated for 1 hour in darkness, washed, and mounted using Vectashield hardest mounting medium with DAPI (Vector Labs H-1500).

IF images were obtained using an LSM780 or LSM880 Zeiss confocal microscope and composite images generated using Fiji. The list of antibodies used is provided in the Key Resources Table as part of STAR Methods.

Quantitative Real-Time Polymerase Chain Reaction—RNA was isolated with the RNeasy Mini Kit (QIAGEN 74104) following manufacturer's protocol and quantified using a NanoDrop Spectrophotometer (ThermoFisher). cDNA synthesis was performed using the TaqMan Reverse Transcription Reagents (ThermoFisher) as indicated by the company. qPCR was then performed using the TaqMan PCR Master Mix (Applied Biosystems) on the StepOne-Plus Real Time PCR System. Data were normalized using the delta Ct method. TaqMan probes used are indicated in the following table:

qRT-PCR TaqMan Probes

Probe	Catalog (ThermoFisher)
CCND1	Hs00765553
MYC	Hs00153408
CTNNB1	Hs00355049
TP63	Hs00978340
Tp63	Mm00495793

QUANTIFICATION AND STATISTICAL ANALYSIS

Statistical methods relevant to each Figure are outlined in the Figure Legend. Statistical anlaysis was performed using GraphPad Prism software version 7–8 (GraphPad, San Diego, CA, USA). Multiple high-power fields were imaged to increase the number (n) of samples used for quantification purposes. Data are presented as the mean ± standard error of the mean (SEM) values. Student's t tests were used to assess statistical significance. Calculated p values are indicated on individual figures.

DATA AND CODE AVAILABILITY

This study did not generate any unique datasets or code.

Supplementary Material

Refer to Web version on PubMed Central for supplementary material.

ACKNOWLEDGMENTS

This work was supported by the UCLA Medical Scientist Training Program (NIH/NIGMS grant GM008042) (C.J.A.), NIH/NCI NRSA Predoctoral F31 Diversity Fellowship F31CA239655 (C.J.A.), the UCLA Eli & Edythe Broad Center of Regenerative (BSCRC) Medicine and Stem Cell Research training grant (C.J.A.), the T32 National Research Service Award in Tumor Cell Biology (CA009056) (C.J.A.), NIH/NCI grant R01CA208303 (B.N.G.), Tobacco Related Disease Research Program (TRDRP) High Impact Pilot Research Award (HIPRA) 26IP-0036 (B.N.G.), TRDRP HIPRA 29IP-0597 (B.N.G.), The UCLA Jonsson Comprehensive Cancer Center (JCCC) STOP Cancer Foundation (B.N.G.), and the UCLA Maximizing Student Development Award (NIH/NIGMS grant R25GM055052 (C.J.P.). We appreciate the UCLA BSCRC Microscopy and Flow Cytometry Cores, the JCCC Flow Cytometry Core, and the UCLA Molecular Screening Shared Resource Core. Statistical analyses were supported by NIH/National Center for Advancing Translational Science (NCATS) UCLA CTSI grant UL1TR000124.

REFERENCES

Akiri G, Cherian MM, Vijayakumar S, Liu G, Bafico A, and Aaronson SA (2009). Wnt pathway aberrations including autocrine Wnt activation occur at high frequency in human non-small-cell lung carcinoma. Oncogene 28, 2163–2172. [PubMed: 19377513]

Au NH, Gown AM, Cheang M, Huntsman D, Yorida E, Elliott WM, Flint J, English J, Gilks CB, and Grimes HL (2004). P63 expression in lung carcinoma: a tissue microarray study of 408 cases. Appl. Immunohistochem. Mol. Morphol 12, 240–247. [PubMed: 15551738]

Caron A, Xu X, and Lin X (2012). Wnt/β-catenin signaling directly regulates Foxj1 expression and ciliogenesis in zebrafish Kupffer's vesicle. Development 139, 514–524. [PubMed: 22190638]

Cole BB, Smith RW, Jenkins KM, Graham BB, Reynolds PR, and Reynolds SD (2010). Tracheal Basal cells: a facultative progenitor cell pool. Am. J. Pathol 177, 362–376. [PubMed: 20522644]

Ekins S, and Bunin BA (2013). The Collaborative Drug Discovery (CDD) database. Methods Mol. Biol 993, 139–154. [PubMed: 23568469]

Fang D, Hawke D, Zheng Y, Xia Y, Meisenhelder J, Nika H, Mills GB, Kobayashi R, Hunter T, and Lu Z (2007). Phosphorylation of beta-catenin by AKT promotes beta-catenin transcriptional activity. J. Biol. Chem 282, 11221–11229. [PubMed: 17287208]

Fang L, Zhu Q, Neuenschwander M, Specker E, Wulf-Goldenberg A, Weis WI, von Kries JP, and Birchmeier W (2016). A small-molecule antagonist of the β-catenin/TCF4 interaction blocks the self-renewal of cancer stem cells and suppresses tumorigenesis. Cancer Res. 76, 891–901. [PubMed: 26645562]

Gerby B, Veiga DF, Krosl J, Nourreddine S, Ouellette J, Haman A, Lavoie G, Fares I, Tremblay M, Litalien V, et al. (2016). High-throughput screening in niche-based assay identifies compounds to target preleukemic stem cells. J. Clin. Invest 126, 4569–4584. [PubMed: 27797342]

Giangreco A, Lu L, Vickers C, Teixeira VH, Groot KR, Butler CR, Ilieva EV, George PJ, Nicholson AG, Sage EK, et al. (2012). β-Catenin determines upper airway progenitor cell fate and preinvasive squamous lung cancer progression by modulating epithelial-mesenchymal transition. J. Pathol 226, 575–587. [PubMed: 22081448]

Haas M, Gómez Vázquez JL, Sun DI, Tran HT, Brislinger M, Tasca A, Shomroni O, Vleminckx K, and Walentek P (2019). ΔN-Tp63 mediates Wnt/β-catenin-induced inhibition of differentiation in basal stem cells of mucociliary epithelia. Cell Rep. 28, 3338–3352.e6. [PubMed: 31553905]

Hegab AE, Ha VL, Attiga YS, Nickerson DW, and Gomperts BN (2012a). Isolation of basal cells and submucosal gland duct cells from mouse trachea. J. Vis. Exp 67, e3731.

Hegab AE, Ha VL, Darmawan DO, Gilbert JL, Ooi AT, Attiga YS, Bisht B, Nickerson DW, and Gomperts BN (2012b). Isolation and in vitro characterization of basal and submucosal gland duct stem/progenitor cells from human proximal airways. Stem Cells Transl. Med 1, 719–724. [PubMed: 23197663]

Hegab AE, Ha VL, Bisht B, Darmawan DO, Ooi AT, Zhang KX, Paul MK, Kim YS, Gilbert JL, Attiga YS, et al. (2014). Aldehyde dehydrogenase activity enriches for proximal airway basal stem cells and promotes their proliferation. Stem Cells Dev. 23, 664–675. [PubMed: 24171691]

Hogan BL, Barkauskas CE, Chapman HA, Epstein JA, Jain R, Hsia CC, Niklason L, Calle E, Le A, Randell SH, et al. (2014). Repair and regeneration of the respiratory system: complexity, plasticity, and mechanisms of lung stem cell function. Cell Stem Cell 15, 123–138. [PubMed: 25105578]

Hong KU, Reynolds SD, Watkins S, Fuchs E, and Stripp BR (2004). Basal cells are a multipotent progenitor capable of renewing the bronchial epithelium. Am. J. Pathol 164, 577–588. [PubMed: 14742263]

Huber AH, and Weis WI (2001). The structure of the beta-catenin/E-cadherin complex and the molecular basis of diverse ligand recognition by beta-catenin. Cell 105, 391–402. [PubMed: 11348595]

Hwang SY, Deng X, Byun S, Lee C, Lee SJ, Suh H, Zhang J, Kang Q, Zhang T, Westover KD, et al. (2016). Direct targeting of β-catenin by a small molecule stimulates proteasomal degradation and suppresses oncogenic Wnt/β-catenin signaling. Cell Rep. 16, 28–36. [PubMed: 27320923]

Inglese J, Auld DS, Jadhav A, Johnson RL, Simeonov A, Yasgar A, Zheng W, and Austin CP (2006). Quantitative high-throughput screening: a titration-based approach that efficiently identifies

biological activities in large chemical libraries. Proc. Natl. Acad. Sci. USA 103, 11473–11478. [PubMed: 16864780]

Ishizumi T, McWilliams A, MacAulay C, Gazdar A, and Lam S (2010). Natural history of bronchial preinvasive lesions. Cancer Metastasis Rev. 29, 5–14. [PubMed: 20112052]

Lyou Y, Habowski AN, Chen GT, and Waterman ML (2017). Inhibition of nuclear Wnt signalling: challenges of an elusive target for cancer therapy. Br. J. Pharmacol 174, 4589–4599. [PubMed: 28752891]

Ma Y, Fan M, Dai L, Kang X, Liu Y, Sun Y, Xiong H, Liang Z, Yan W, and Chen K (2015). Expression of p63 and CK5/6 in early-stage lung squamous cell carcinoma is not only an early diagnostic indicator but also correlates with a good prognosis. Thorac. Cancer 6, 288–295. [PubMed: 26273374]

Malleske DT, Hayes D Jr., Lallier SW, Hill CL, and Reynolds SD (2018). Regulation of human airway epithelial tissue stem cell differentiation by β-catenin, P300, and CBP. Stem Cells 36, 1905–1916. [PubMed: 30171668]

Montoro DT, Haber AL, Biton M, Vinarsky V, Lin B, Birket SE, Yuan F, Chen S, Leung HM, Villoria J, et al. (2018). A revised airway epithelial hierarchy includes CFTR-expressing ionocytes. Nature 560, 319–324. [PubMed: 30069044]

Ooi AT, Mah V, Nickerson DW, Gilbert JL, Ha VL, Hegab AE, Horvath S, Alavi M, Maresh EL, Chia D, et al. (2010). Presence of a putative tumor-initiating progenitor cell population predicts poor prognosis in smokers with non-small cell lung cancer. Cancer Res. 70, 6639–6648. [PubMed: 20710044]

Paul MK, Bisht B, Darmawan DO, Chiou R, Ha VL, Wallace WD, Chon AT, Hegab AE, Grogan T, Elashoff DA, et al. (2014). Dynamic changes in intracellular ROS levels regulate airway basal stem cell homeostasis through Nrf2-dependent Notch signaling. Cell Stem Cell 15, 199–214. [PubMed: 24953182]

Plasschaert LW, Žilionis R, Choo-Wing R, Savova V, Knehr J, Roma G, Klein AM, and Jaffe AB (2018). A single-cell atlas of the airway epithelium reveals the CFTR-rich pulmonary ionocyte. Nature 560, 377–381. [PubMed: 30069046]

Rhee J, Buchan T, Zukerberg L, Lilien J, and Balsamo J (2007). Cables links Robo-bound Abl kinase to N-cadherin-bound beta-catenin to mediate Slit-induced modulation of adhesion and transcription. Nat. Cell Biol 9, 883–892. [PubMed: 17618275]

Rock JR, Onaitis MW, Rawlins EL, Lu Y, Clark CP, Xue Y, Randell SH, and Hogan BL (2009). Basal cells as stem cells of the mouse trachea and human airway epithelium. Proc. Natl. Acad. Sci. USA 106, 12771–12775. [PubMed: 19625615]

Schoch KG, Lori A, Burns KA, Eldred T, Olsen JC, and Randell SH (2004). A subset of mouse tracheal epithelial basal cells generates large colonies in vitro. Am. J. Physiol. Lung Cell. Mol. Physiol 286, L631–L642. [PubMed: 12959927]

Tammela T, Sanchez-Rivera FJ, Cetinbas NM, Wu K, Joshi NS, Helenius K, Park Y, Azimi R, Kerper NR, Wesselhoeft RA, et al. (2017). A Wnt-producing niche drives proliferative potential and progression in lung adenocarcinoma. Nature 545, 355–359. [PubMed: 28489818]

Ueda M, Gemmill RM, West J, Winn R, Sugita M, Tanaka N, Ueki M, and Drabkin HA (2001). Mutations of the beta- and gamma-catenin genes are uncommon in human lung, breast, kidney, cervical and ovarian carcinomas. Br. J. Cancer 85, 64–68. [PubMed: 11437403]

Walentek P, Beyer T, Thumberger T, Schweickert A, and Blum M (2012). ATP4a is required for Wnt-dependent Foxj1 expression and leftward flow in Xenopus left-right development. Cell Rep. 1, 516–527, 516–527. [PubMed: 22832275]

Walentek P, Beyer T, Hagenlocher C, Müller C, Feistel K, Schweickert A, Harland RM, and Blum M (2015). ATP4a is required for development and function of the Xenopus mucociliary epidermis - a potential model to study proton pump inhibitor-associated pneumonia. Dev. Biol 408, 292–304. [PubMed: 25848696]

Wang BY, Gil J, Kaufman D, Gan L, Kohtz DS, and Burstein DE (2002). P63 in pulmonary epithelium, pulmonary squamous neoplasms, and other pulmonary tumors. Hum. Pathol 33, 921–926. [PubMed: 12378518]

Zemke AC, Teisanu RM, Giangreco A, Drake JA, Brockway BL, Reynolds SD, and Stripp BR (2009). beta-Catenin is not necessary for maintenance or repair of the bronchiolar epithelium. Am. J. Respir. Cell Mol. Biol 41, 535–543. [PubMed: 19213872]

Highlights

- A dysregulated Wnt/β-catenin axis in human lung premalignancy can be modeled *in vitro*
- High-throughput drug screening identifies the Wnt/β-catenin inhibitor WIC1
- Low-dose treatment with WIC1 promotes differentiation to the ciliated cell fate
- WIC1 acts to repress phosphorylation of β-catenin^{Y489} and *Tp63* expression

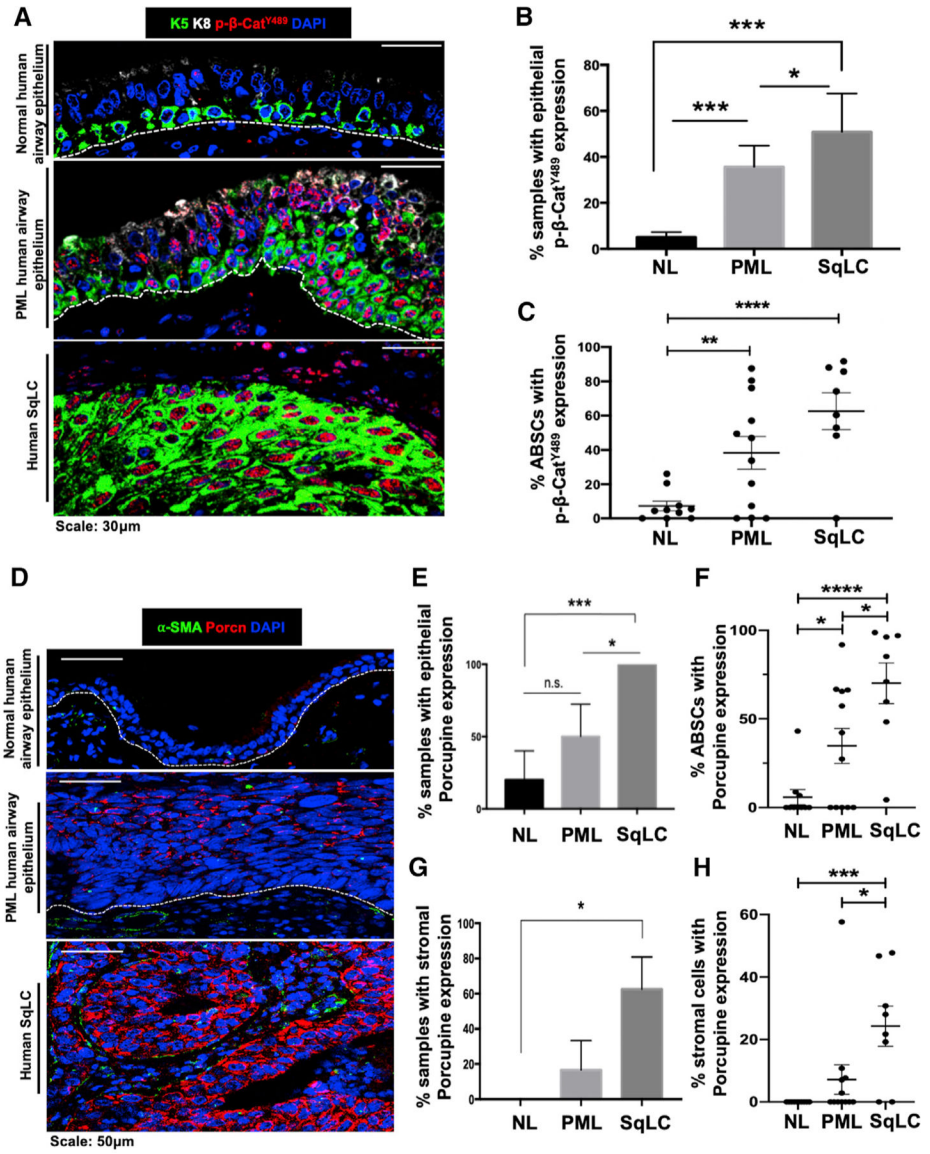

Figure 1. Emergence of Dysregulated Wnt/p-β-Catenin^{Y489} Signaling Axis in Stepwise Progression to Human SqLC

(A) IF images of p-β-catenin^{Y489} in human normal (NL) airway epithelium, premalignant lesions (PMLs), and squamous lung cancer (SqLC) patient samples.

(B) Quantification of percentage of human NL, PML, and SqLC samples with positive epithelial p-β-catenin^{Y489} expression. Three fields were quantified per patient.

(C) Quantification of percentage of ABSCs with nuclear p-β-catenin^{Y489} expression during stepwise progression to SqLC. Three fields were quantified per patient.

(D) IF images of Porcupine in human normal airway epithelium, PMLs, and SqLC patient samples.

(E) Quantification of percentage of human NL, PML, and SqLC samples with positive epithelial Porcupine expression. Three fields were quantified per patient.

(F) Quantification of percentage of ABSCs with Porcupine expression during progression to SqLC. Three fields were quantified per patient.

(G) Quantification of percentage of human NL, PML, and SqLC samples with positive Porcupine expression in the stromal compartment. Three fields were quantified per patient.
(H) Quantification of percentage of stromal cells with Porcupine expression during progression to SqLC. Three fields were quantified per patient.
*p < 0.05, **p < 0.01, ***p < 0.001, and ****p < 0.0001; n.s., not significant by Student's t test. All error bars represent mean ± SEM.

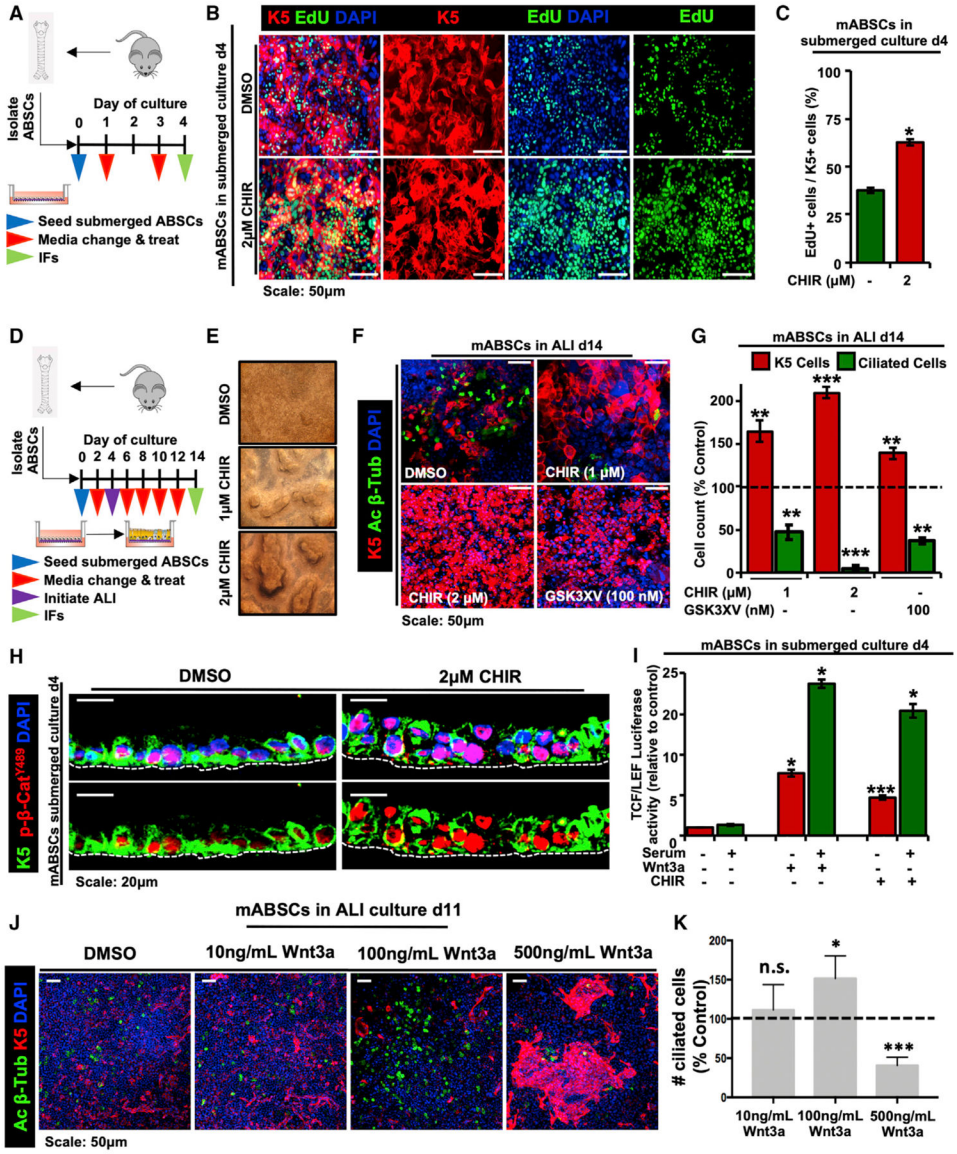

Figure 2. Dysregulated ABSC Homeostasis Is Controlled by Perturbations in Canonical Wnt Signaling *In vitro*

(A) Schema outlining seeding and treatment of mABSCs under submerged conditions with DMSO or CHIR.

(B) IF images of mABSC proliferation *in vitro* under submerged conditions on day 4 treated with DMSO or CHIR using the click-iT EdU assay.

(C) Quantification of proliferating $K5^{+}$ EdU^{+} mABSCs under CHIR- versus DMSO-treated conditions *in vitro*. Five fields of each treatment were used for quantification.

(D) Schema outlining seeding and treatment of mABSCs under submerged and ALI conditions with DMSO or CHIR.

(E) Bright-field images of mABSCs under ALI conditions for 11 days treated with CHIR *in vitro*.

(F) IF images of mABSCs under ALI culture conditions for 14 days treated *in vitro* with two independent GSK3β inhibitors CHIR and GSK3XV. Acetylated β-tubulin (Ac β-Tub) is a marker of ciliated cells.

(G) Quantification of ABSCs and ciliated cells from mABSC cultures under ALI conditions for 14 days treated with CHIR and GSK3XV. Data are normalized DMSO-treated controls, indicated by the dotted line. Five fields of each treatment were used for quantification.

(H) IF images of mABSC submerged cultures treated with CHIR for 4 days for p-β-catenin^{Y489}.

(I) Bar graph depicting TCF/LEF activity of mABSCs treated with recombinant mouse Wnt3a or CHIR, measured by a luciferase reporter.

(J) IF images of mABSCs under ALI conditions for 11 days treated with varying concentrations of recombinant mouse Wnt3a *in vitro*.

(K) Quantification of ciliated cells from mABSC cultures under ALI conditions for 11 days treated with varying concentrations of Wnt3a. Data are normalized DMSO-treated controls, indicated by the dotted line. Three to six fields of each treatment were used for quantification (n = 3–6).

*p < 0.05, **p < 0.01, and ***p < 0.001 by Student's t test. All error bars represent mean ± SEM.

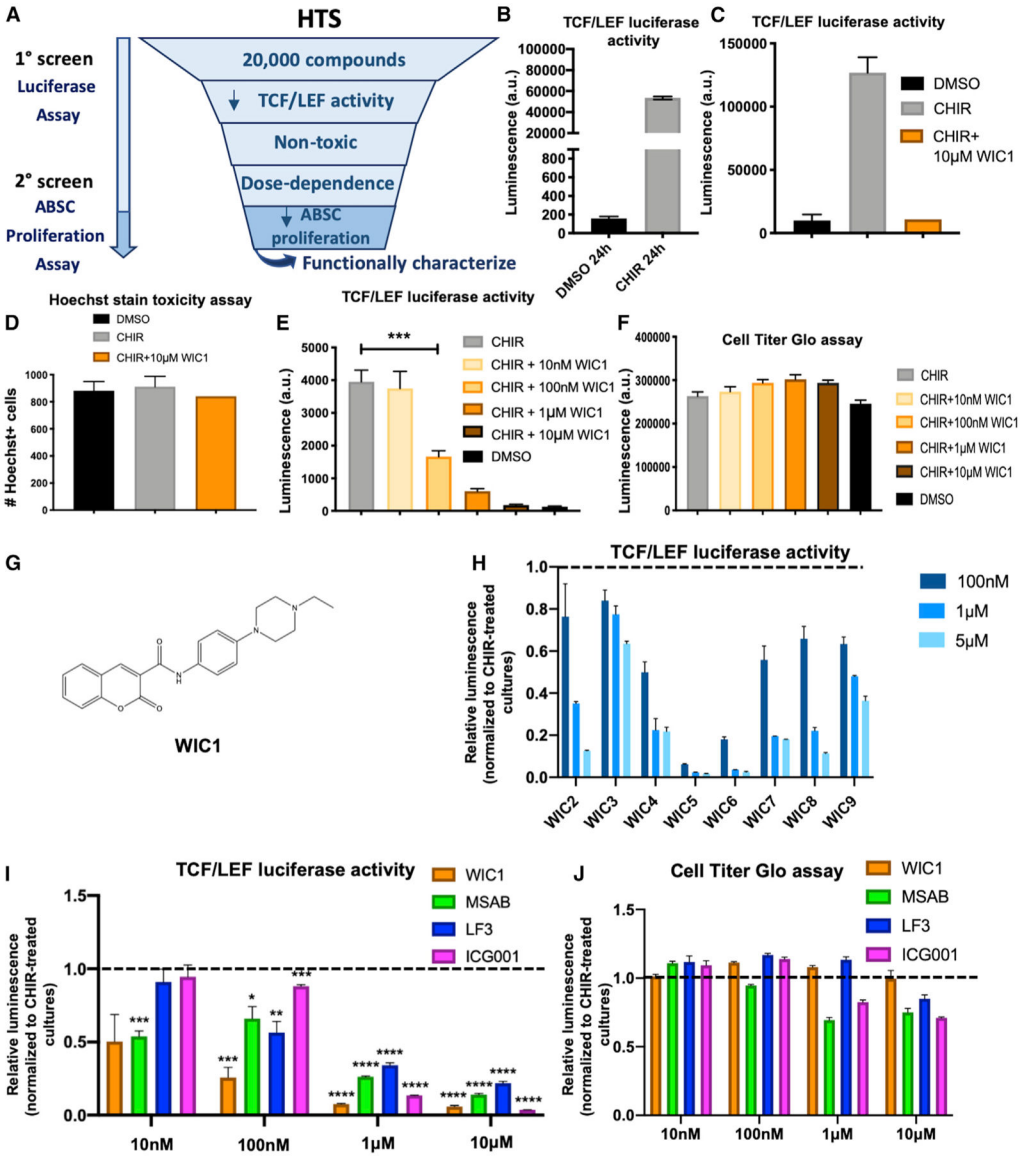

Figure 3. High-Throughput Drug Screening Identifies a Small-Molecule Inhibitor of Canonical Wnt Signaling

(A) High-throughput screen (HTS) schema to identify small molecule inhibitors of Wnt signaling.

(B) Bar graph representing BEAS2B TCF/LEF luciferase reporter activity treated with DMSO or CHIR for 24 h used for HTS.

(C) Bar graph representing BEAS2B TCF/LEF luciferase reporter activity treated with DMSO, CHIR, or CHIR + WIC1 after 24 h from HTS.

(D) Bar graph representing percentage of viable, nontoxic BEASB cells measured by Hoechst staining treated with DMSO, CHIR, or CHIR + WIC1 from HTS.

(E) Bar graph representing BEAS2B TCF/LEF luciferase reporter activity treated with DMSO, CHIR, or CHIR with varying concentrations of WIC1 for 24 h.

(F) Bar graph representing CellTiter-Glo assay in BEAS2B cells treated with DMSO, CHIR, or CHIR with varying concentrations of WIC1.

(G) Structure of WIC1.
(H) Bar graph representing BEAS2B TCF/LEF luciferase reporter activity treated with CHIR and varying concentrations of WIC2–WIC9 from SAR studies. Data are normalized to CHIR-treated cultures, indicated by the dotted line.
(I) Bar graph representing BEAS2B TCF/LEF luciferase reporter activity treated for 24 h with 5 μM CHIR or 5 μM CHIR plus indicated concentrations of WIC1, MSAB, LF3, or ICG001. Data are normalized to CHIR-treated cultures, indicated by the dotted line.
(J) Bar graph representing the CellTiter-Glo assay in BEAS2B cells treated for 24 h with 5 μM CHIR or 5 μM CHIR plus indicated concentrations of WIC1, MSAB, LF3, or ICG001. Data are normalized to CHIR-treated cultures, indicated by the dotted line (n = 3–6).
*p < 0.05, **p < 0.01, ***p < 0.001, and ****p < 0.0001 by Student's t test. All error bars represent mean ± SEM.

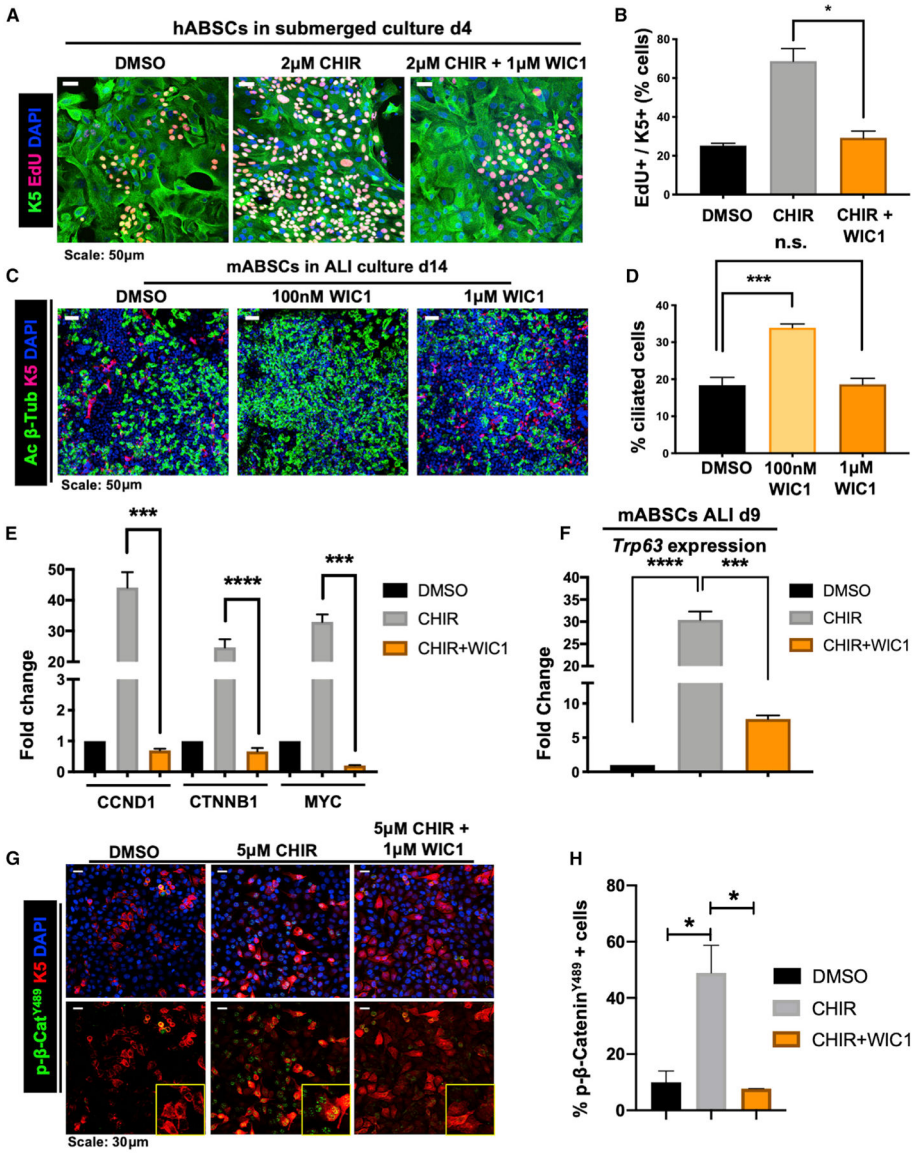

Figure 4. WIC1 Inhibits Wnt-Induced ABSC Hyperproliferation, Promotes Ciliated Cell Differentiation, and Acts by Decreasing Nuclear p-β-Catenin^{Y489}

(A) IF images of mABSCs *in vitro* under submerged conditions on day 4 treated with DMSO, CHIR, or CHIR+WIC1 using click-iT EdU assay.

(B) Quantification of K5+ EdU+ mABSCs under submerged conditions on day 4 treated with DMSO, CHIR, or CHIR+WIC1. 3 fields of each treatment used for quantification.

(C) IF images of mABSCs *in vitro* under ALI culture conditions for 14 days treated with DMSO or indicated concentrations of WIC1.

(D) Quantification of percentage of ciliated cells from mABSC cultures under ALI conditions for 14 days treated with DMSO or indicated concentrations of WIC1. Four fields of each treatment were used for quantification.

(E) Bar graph representing qPCR data assessing mRNA expression of *CCND1*, *CTNNB1*, and *MYC* in BEAS2B cells treated with DMSO, 5 μM CHIR, or 5 μM CHIR + 1 μM WIC1 for 48 h.

(F) Bar graph representing qPCR data assessing mRNA expression of *Trp63* in mABSCs treated with DMSO, 1 μM CHIR, or 1 μM CHIR + 1 μM WIC1 on ALI culture day 9.
(G) IF images for p-β-catenin^{Y489} from BEAS2B cells treated with DMSO, 5 μM CHIR, or 5 μM CHIR + 1 μM WIC1 for 24 h. Yellow boxes show magnified inlets of the indicated treatment.
(H) Quantification of percentage of p-β-catenin^{Y489+} BEAS2B cells treated with DMSO, 5 μM CHIR, or 5 μM CHIR + 1 μM WIC1 for 24 h. Three fields of each treatment were used for quantification (n = 3–6).
*$p < 0.05$, **$p < 0.01$, ***$p < 0.001$, and ****$p < 0.0001$ by Student's t test. All error bars represent mean ± SEM.

KEY RESOURCES TABLE

REAGENT or RESOURCE	SOURCE	IDENTIFIER
Antibodies		
Goat anti-mouse TROP2-APC	R&D	Cat# AF1122; RRID:AB_2205662
Rat anti-mouse ITGA6-PE	BioLegend	Cat# 313611; RRID:AB_893374
Rabbit Keratin 5	Covance	Cat # PRB-160P; RRID:AB_291581
Rat Keratin 8	DSHB	Cat# TROMA-I; RRID:AB_531826
Mouse Acetylated b-Tubulin	Sigma	Cat# T7451; RRID:AB_609894
Rabbit Porcupine	Abcam	Cat# ab105543; RRID:AB_10860951
Mouse p-β-catenin^{Y489}	DSHB	Cat# PY489-B-catenin; RRID:AB_10144551
Rabbit p-β-catenin^{S33,S37,T41}	Cell Signaling Technology	Cat# 9561T; RRID:AB_331729
Rabbit p-β-catenin^{S654}	DSHB	Cat# PY654-B-catenin; RRID:AB_2088265
Rabbit p-β-catenin^{Y142}	Abcam	Cat# ab27798; RRID:AB_725969
Rabbit p-β-catenin^{S552}	Cell Signaling Technology	Cat# 9566S; RRID:AB_1031116
Mouse α-SMA	Sigma	Cat# A2547; RRID:AB_476701
Goat anti-Rabbit IgG (H+L) Highly Cross-Adsorbed Secondary Antibody, Alexa Fluor 594	ThermoFisher	Cat# A-11037; RRID:AB_2534095
Goat anti-Mouse IgG (H+L) Highly Cross-Adsorbed Secondary Antibody, Alexa Fluor 488	ThermoFisher	Cat# A-11029; RRID:AB_138404
Goat anti-Chicken IgY (H+L) Secondary Antibody, Alex Fluor 488	ThermoFisher	Cat# A-11039; RRID:AB_142924
Goat anti-Rat IgG (H+L) Cross-Adsorbed Secondary Antibody, Alexa Fluor 647	ThermoFisher	Cat# A-21247; RRID:AB_141778
Biological Samples		
Human bronchiolar airway tissue specimens	Ronald Reagan UCLA Medical Center	N/A
Chemicals, Peptides, and Recombinant Proteins		
CHIR99021	Tocris	Cat# 4423
GSK3XV	Millipore Sigma	Cat# 361558
Recombinant mouse Wnt3a	R&D Systems	Cat# 1324-WN
Dispase	Corning	Cat# 354235
Collagen type I	Corning	Cat# 354249
HEPES	Sigma	Cat# H0887
Sodium Bicarbonate	Life Technologies	Cat# 25080–094
L-glutamine	Invitrogen	Cat# 35050–061
Insulin	Sigma	Cat# I6634
Transferrin	Sigma	Cat# T5391
Cholera Toxin	Sigma	Cat# C8052
Epidermal Growth Factor (EGF)	Corning	Cat# 354001
Bovine Pituitary Extract	Invitrogen	Cat# 13028–014
Fetal Bovine Serum	ThermoFisher	Cat# SH3008803HI
Bovine Serum Albumin	ThermoFisher	Cat# BP9706
Retinoic Acid	Sigma	Cat# R2625
MSAB	Sigma	Cat# SML1726

REAGENT or RESOURCE	SOURCE	IDENTIFIER
LF3	Sigma	Cat# SML1752
ICG001	Tocris	Cat# 4505
Critical Commercial Assays		
Click-iT EdU Incorporation Assay Kit	Invitrogen	Cat# C10337
Experimental Models: Organisms/Strains		
Mouse: C57BL/6J	The Jackson Laboratory	JAX Stock# 000664
Software and Algorithms		
GraphPad Prism 7	GraphPad Software	RRID:SCR_002798
Fiji	ImageJ	RRID:SCR_002285